Automation in Construction 140 (2022) 104334

Contents lists available at ScienceDirect

Automation in Construction

journal homepage: www.elsevier.com/locate/autcon

Geometric and semantic point cloud data for quality control of bridge girder reinforcement cages

Gabrielle Hodge, Joseph M. Gattas *

School of Civil Engineering, The University of Queensland, Australia

ARTICLE INFO

Keywords:
LiDAR
Bridge girder reinforcement
Automatic rebar measurement
Semantic enrichment
Quality control

ABSTRACT

The reinforcement of bridge girders is critical to ensuring adequate strength, serviceability, and durability. Achievement of these criteria is assessed by quality control processes conducted throughout construction. This study explores two methods for processing point clouds of bridge girder reinforcement cages, to output positional and dimensional data utilised for quality control. An extended slicing method is first employed to enable the segmentation and classification of 3D rebar within complex bridge girder reinforcement cages. A semantic enrichment method is then used to infer data regarding the the individual rebar and rebar shapes, and improve the accuracy of prior identified information. The proposed algorithms were tested on two point clouds of bridge girder reinforcement cages collected on-site. Positional results, spacing and orientation, reported an average error of less than 2 mm and 0.1°. An average error of 5% was reported for the dimensional length of rebar, decreasing to 1% following the semantic enrichment algorithm. The basis of the presented methodology, including the identification, separation, and grouping for distinct placements of rebar (longitudinal, vertical, and transverse) can be extended for application to other common reinforcement cage archetypes.

1. Introduction

Bridge assets represent a major component of road network investment and decision making [8,43]. To ensure bridge elements meet design specifications and long-term performance requirements, they are subject to stringent quality control (QC) processes, following guidelines published by asset owners and governing bodies, such as [19,20,49] in Australia, [5] in the United States of America, and [11] in Europe. In reinforced concrete structural elements, mandated QC checks and inspections are typically conducted manually by experienced trained personnel. Items assessed may include the type, amount and location of reinforcement, prestress strand, and post-tensioning ducts; or concrete cover, grade, and compaction [14,15,19,49].

Remote sensing technologies are being explored for their potential to augment current inspection practices with a rich and reliable spatial data record [33,47,56]. Light Detection and Ranging (LiDAR) and photogrammetry remote sensing technologies capture detailed geometric information in the form of point cloud data (PCD) [33,53]. This can be post-processed to provide a comprehensive digital record of the environment, for example as a labelled PCD, a generated geometric 3D model, or a semantically enriched 3D model [3,37,54,56]. Suggested remote sensing applications for QC and inspection in architecture, engineering and construction industries include measuring deflections and clearances of structures [12,48], assessing code compliance of scaffold structures [54] and checking geometrical quality of precast concrete elements [45,58]. Recent studies on the use of LiDAR have explored dimensional quality assurance of reinforcement cages, primarily in slabs and walls [28,34,57]. A decrease of approximately 45% in time required to inspect reinforcement cages was demonstrated by [1] when tablet-based 3D models were used compared with manual inspections.

This paper aims to demonstrate the feasibility and future work required for the application of LiDAR to quality control of bridge girder reinforcement cages. A review of the existing literature is presented in Section 2. A description of the methodology of the PCD processing and semantic enrichment algorithms is contained in Section 3. The implementation of these algorithms is presented in Section 4. Method validation and results are contained in Section 5, with discussion on the feasibility of the proposed LiDAR-based QC in Section 6.

* Corresponding author.
E-mail address: j.gattas@uq.edu.au (J.M. Gattas).

https://doi.org/10.1016/j.autcon.2022.104334
Received 20 December 2021; Received in revised form 6 April 2022; Accepted 5 May 2022
Available online 20 May 2022
0926-5805/© 2022 Elsevier B.V. All rights reserved.

2. Literature review

2.1. Bridge girder and reinforcement cages characteristics

There are over 37,000 public road bridges in Australia, with approximately 75% of highway bridges constructed with concrete [8]. The representative proportion of concrete bridges is similarly high in the United Kingdom at 80% [25] and in the United States at 68% [52]. A typical beam and slab bridge, shown in Fig. 1, consists of prestressed concrete girders spanning between in-situ reinforced concrete headstocks, supported on concrete piers and piles or footings. This bridge type is often considered appropriate for medium length spans, in the range of 11 m to 45 m [21,26].

The arrangement of reinforcement within a concrete element is determined by geometric and loading requirements. Slabs, spanning either one or two directions, have an upper limit on the span to depth ratio of approximately 20:1, with maximum spans around 15 m for solid slab bridges [9,26]. Slab reinforcement cages are typically reinforced longitudinally and transversely, with at least two sets of perpendicular faces, Fig. 2a [40]. A span to depth ratio of between 16:1 and 20:1 is common for girders in beam and slab bridges, with maximum economical spans approximately 35 m [9,26]. Girder reinforcement cages are reinforced in all directions at both ends and primarily in the vertical and longitudinal direction at midspan, Fig. 2b, with many profiles containing non-perpendicular faces [7,24,26,40].

Despite the seemingly complex geometric design space, the arrangement of rebar within bridge girders will generally comply with standard reinforcement details of asset owners or construction preferences of precasters. In Queensland, these are published by the Department of Transport and Main Roads (DTMR) as standard drawings and details [16,21]. Reinforcement cages share certain features across all standard girders, which are noted here as of later relevance to the algorithm developed in this paper.

With reference to Fig. 3, longitudinal reinforcement extends the full length of the reinforcement cage ①, with rebar laps having a cross-sectional offset of one diameter ②. The vertical and horizontal rebar are arranged in *sets*, spanning approximately the maximum depth (vertical direction) and width (transverse direction) of the girder ③. Each set may be splayed in plan, and there is always a clear span of longitudinal reinforcement between discrete sets to comply with minimum spacing requirements, discussed in the next section. The geometry of individual rebars must additionally comply with standard size, identification, and detailing conventions, to support standardisation across different bridge girders. Rebar in DTMR projects is standardised as one of 90 named bar shapes ⑤, published in [18] with pre-defined hook, cog, and bend dimensions for typical bar diameters. Typical rebar are near-circular with diameters between 10 mm and 36 mm, in size increments of 2 mm or 4 mm [50]. The use of non-standard rebar shapes is allowed, provided details are specified on project drawings [15].

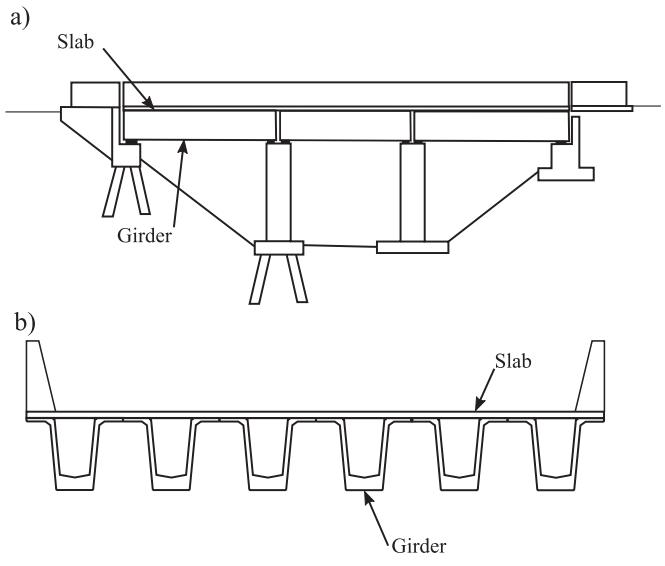

Fig. 1. Typical beam and slab bridge adapted from [7]: a) elevation of beam and slab bridge, and b) typical section.

2.2. Quality control and dimensional tolerances

The responsibility for QC of concrete bridge elements is shared by all entities involved, with internal inspections, mandated inspections, and verification processes conducted throughout construction [6,14,44]. The goal of these QC processes is to limit discrepancies between the as-built and as-designed element, while minimising the need for costly and time-consuming rework or repairs during construction [6]. For economical and efficient construction, it is unrealistic for the as-built element to exactly adhere to the as-designed element, so allowable tolerances are defined [44] to account for deviation due to human error or limitation. These tolerances are tightly controlled and documented to ensure strength, durability, and constructibility performance compliance [14,44].

For reinforcing steel in concrete, QC can encompass rebar diameter, shape, cover to reinforcement, and overall element geometry. These are assessed against positional tolerances, including spacing and skew of rebar, and dimensional tolerances, such as overall rebar length [14,15,19,49]. Examples of positional and dimensional tolerances of reinforcement for concrete bridge projects are summarised in Table 1 [17,19,49].

2.3. LiDAR applications in reinforced and precast concrete

LiDAR scanners are increasingly used in Architecture, Engineering and Construction (AEC) industries for the remote collection of environmental spatial data [13,53]. With regards to LiDAR scanning of concrete structures, recent research has developed a range of automated processing techniques for point cloud segmentation and object recognition [33,53,56]. Segmentation refers to the process of grouping points based on shared characteristics, for example segmenting a bridge scan into discrete structural components using geometric heuristics [37] or segmenting a masonry wall scan into mortar and individual blocks using LiDAR intensity values [48]. Object recognition involves labelling the segmented group to associate each group with a predefined class [13,53]. For AEC industries, a number of studies have implemented knowledge-based approaches for object recognition, such as predefined rules for the identification of walls, ceilings, floors, and openings [2]; or to differentiate between scaffold platform floors, toe boards, and guardrails [55]. A knowledge-based approach to region growing was implemented by [46] for the generation of semantic floor maps, where segments meeting geometric and semantic criteria were merged. Segmentation and recognition processes were intertwined by [37], where a 3D slicing algorithm was developed using a knowledge-based approach to segment and identify bridge components. A 2D slicing algorithm was similarly used by [27] for the identification of boundary points within façades, with vertical and horizontal slices utilised to identify horizontal and vertical discontinuities. 1D slicing algorithms were demonstrated to be effective for the identification of cylindrical pillars and utility poles by [38,39], with circle fitting conducted on multiple slices along a vertical axis. PCD slicing has also been explored as an effective method to decompose and process complex PCDs [42], with segmentation and subsequent merging of identified objects from PCD slices.

Studies have identified numerous potential benefits from incorporating the use of LiDAR into QC processes. Time and cost savings from the application of LiDAR for surface flatness QC were reported by [45]. LiDAR measurement accuracy was demonstrated to be sufficient for

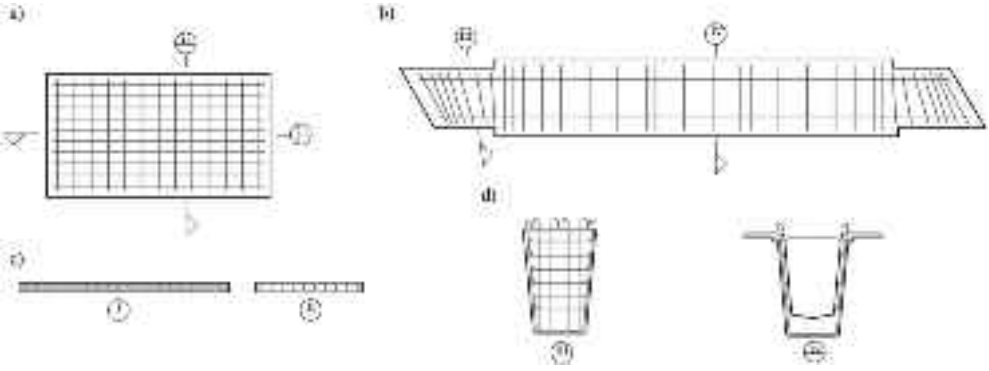

Fig. 2. Typical slab and girder reinforcement: a) Plan - slab, b) Plan - girder, c) Sections - slab, and d) Sections - girder.

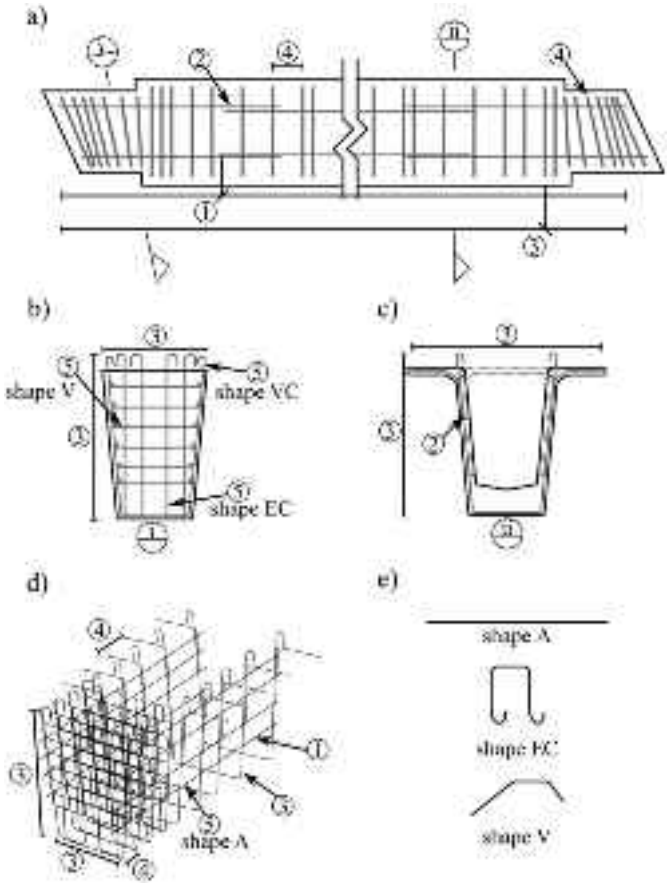

Fig. 3. Bridge girder reinforcement cage characteristics: a) Plan b) Section - endblock, c) Section - midspan, d) Isometric, and e) standard bar shapes.

automated dimensional QC of precast panels, as scanned in both laboratory environments [31] and on-site [32]. The location of embedded items and cutouts within these panels was additionally assessed, with data used to generate accurate as-built 3D models, which also allowed for the alignment and optimised placement of concrete elements on-site [58]. Accurate as-built data records can also assist with works after construction, for example rebar diameter and intersection locations were determined from PCDs in [3,23]. A corresponding generated 3D model identified unreinforced regions within the concrete slab, to later inform safe drill locations.

Several processing methods have been developed for reinforcement cage PCDs, to determine the spacing, location, and diameter of rebar within slab or deck plate elements [23,34,35,57]. Colour and geometric

Table 1
Tolerances and requirements for steel reinforcement in concrete bridges.

Rebar	Tolerance	Requirement
Overall dimension	± 5 mm specified	–
Position in cross section	± 10 mm	–
Position of rebar ends	± 50 mm	–
Spacing of rebar	–	≥ 1.5 × aggregate size, ≥ rebar diameter
Set spacing	± 10% of nominated spacing ≥ 15 mm	≥ 90 mm
Set skew	± $3d_b$	–
Longitudinal rebar bends	–	$5d_b$
Transverse rebar bends	–	$5d_b$
Vertical rebar bends	–	$4d_b$

heuristics were used by [23] in a method to isolate exposed rebar from a concrete deck plate PCD, subsequently allowing rebar number and location to be quantified. A RANSAC algorithm was used to identify locations of rebar with a known diameter [34], to then calculate rebar spacing. This was extended using a machine learning approach to also allow identification without prior knowledge of rebar diameters, albeit with an increase in processing time from 3.53 min [34] to 44.5 min [35]. Improved accuracy in the assessment of rebar diameter was reported when the results of the discrete segments were combined into the individual rebar.

The quality of the point cloud data, including accuracy, density, and completeness, is central to the efficacy of using LiDAR to provide meaningful QC information [47,56]. It is of particular importance for reinforcement steel QC, as the 1 mm to 10 mm measurement accuracy attainable by terrestrial LiDAR scanners is comparable to the difference of 2 mm between different rebar sizes [33,53]. The effect of noise, erroneous points in the PCD, can also be magnified when identifying small objects such as rebar [10,36]. To minimise this, rebar processing typically includes a noise removal step [28,34,35,41,57]. Density has also been shown as critical for valid interpretation and assessment of the captured data, for example a decrease in PCD density was shown to correlate with increased error in measurement of rebar spacing [34] and a decreased accuracy of rebar diameter identification and spacing [35]. The presence of multiple layers of rebar within reinforcement cages was identified as a cause of occlusion by [34], with densely-reinforced full-scale reinforcement cages noted as more likely to suffer a greater degradation of PCD compared to the study PCD of a lightly-reinforced laboratory scale reinforcement cage. Similarly, increasing occlusion, due to increased reinforcement density, was correlated with decreasing accuracy when measuring rebar positions [57].

The influence of laboratory conditions compared to on-site has been

reported in the progression of concrete QC studies [31,32]. Laboratory results showed an average dimensional error of 1.97 mm and positional error of 1.85 mm [31], compared to on-site errors of 3.68 mm (dimensional) and 3.60 mm (positional) [32]. For reinforcement cages, PCDs obtained in laboratory environments were used to quantify spacing and diameters of rebar [23,34,35]. PCDs collected on-site have been used to identify the presence of rebars within reinforcement cages [28] and spacing of exposed rebar [57].

2.4. Contribution

Twin challenges are encountered in considering PCD classification, processing, and QC methods suited for bridge girder reinforcement cages. First, their dense and irregularly shaped reinforcement forms a complex non-rectilinear topology, although one that conforms to a regulated, known set of parameters and constraints. Second, small-diameter and multi-layered reinforcement bars with multiple angles will potentially generate significant noise and occlusion when scanned.

The existing literature has not yet explored the processing of LiDAR point clouds for objective and consistent measurement of dimensional and positional QC parameters for complex rebar arrangements, such as those used for bridge girders. Additionally, knowledge-based semantic enrichment of PCD data is yet to be applied to bridge reinforcement cages, despite their importance as a public infrastructure asset class. To address the above knowledge gap, this study will extend proven slicing methods to segment and classify 3D rebar within complex bridge girder reinforcement cages and explore the efficacy of semantic enrichment for improved classification and QC. These methods will be applied to PCDs obtained on-site to further assess the practicality of these current methods and technology for industry application.

3. Methodology

3.1. Overview

This paper proposes a knowledge-based classification algorithm for the automated processing of bridge girder reinforcement cage point cloud data, including extraction of key measures required for reinforcement QC. These measures include the length, diameter, and arrangement of longitudinal rebar and rebar sets, as well as identification and semantic labelling of individual bar shapes.

The overall workflow is shown in Fig. 4 and comprises two methods. The first method extends existing slicing approaches for rebar object identification, with top-down segmentation of an input bridge girder PCD, Fig. 4a-b. A novel semantic enrichment method is then developed with bottom-up data grouping of rebar objects and reconstruction into labelled individual bars, Fig. 4c-d. The two methods are developed from knowledge of standard girder reinforcement and rebar shape characteristics, respectively. The employed knowledge domain is as illustrated in Fig. 3 and summarised as the following rules for rebar identification:

1. Rebar is either present in sets or spanning longitudinally.
2. Rebar sets span the width and height of the cross section, with a near-vertical orientation that may rotate in plan along along the length of the reinforcement cage. Sets are placed discretely with a minimum clear spacing of approximately 90 mm centres.
3. Longitudinal rebar extends the length of the reinforcement cage and may be comprised of multiple lapped rebar. Cross sections between rebar sets contain only longitudinal rebar and any one longitudinal rebar will be present in multiple cross sections.
4. Rebar have an approximately circular cross section with nominal diameter (ϕ) commonly between 10 mm and 40 mm. Permissible tolerances allow a diameter variation of up to 10% for each rib in the surface profile. A tolerance on the mass per unit length of rebar, specified as ±4.5% mass per metre length, also allows for a maximum of 4.5% variation in total cross-sectional area.
5. Rebar will conform to a standardised or specified bar shape.

3.2. Slicing method - top down segmentation for rebar object identification

The first processing method receives raw point cloud data as an input and returns longitudinal, vertical, and transverse rebar objects as an output, with identified bar quantities, diameters, and centreline points. It is developed as a top-down classification approach using a recursive slicing algorithm for segmentation and evaluation at increasing levels of detail. This method is an extension of the slicing approaches discussed in Section 2.3, accounting for the 3D placement and direction of rebar, and the non-orthogonality of bridge girder reinforcement cages. The workflow is shown in Fig. 5 and includes four stages: preprocessing; bar set detection; longitudinal bar identification; and vertical and transverse bar identification. The following nomenclature has been used to define the parameters for rebar identification: point density γ, centre point (in the relevant 2D plane) O, distance in the global x, y, and z-axes as Δx, Δy, and Δz. The subscripts i and j differentiate between separate occurrences of objects, while l, v, and t identify longitudinal, vertical and transverse objects respectively.

3.2.1. Preprocessing

To minimise the influence of noise, the raw point cloud data is first cleaned. Initial cleaning is conducted from LiDAR intensity values, which are a measure of the reflectance of the point, based on the scanner characteristics, target properties, environmental conditions, and range [29,30]. In the case of reinforcement cage scan data, variation of these parameters is expected to be minimal, allowing outlying LiDAR intensity values to be attributed to noise, items other than rebar, or erroneous points which can be removed from the point cloud with minimal loss of information. To remove outliers without over-cleaning the point cloud, points here are removed with an intensity greater or less than three standard deviations from the mean intensity. Additional noise associated with small cylindrical objects, such as rebar, has been identified as characterised by points forming a 2D plane [51]. To identify and remove any regions corresponding to this type of noise, the point cloud is discretised into a 3D grid; any grid cell not containing points distributed across all three axes is removed.

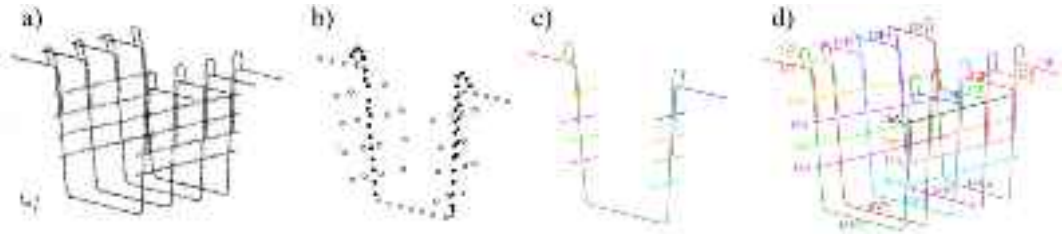

Fig. 4. Methodology: a) PCD input, b) slicing method for rebar object identification, c) semantic enrichment method for bar shape identification, and d) output reinforcement cage with individual bar reconstruction.

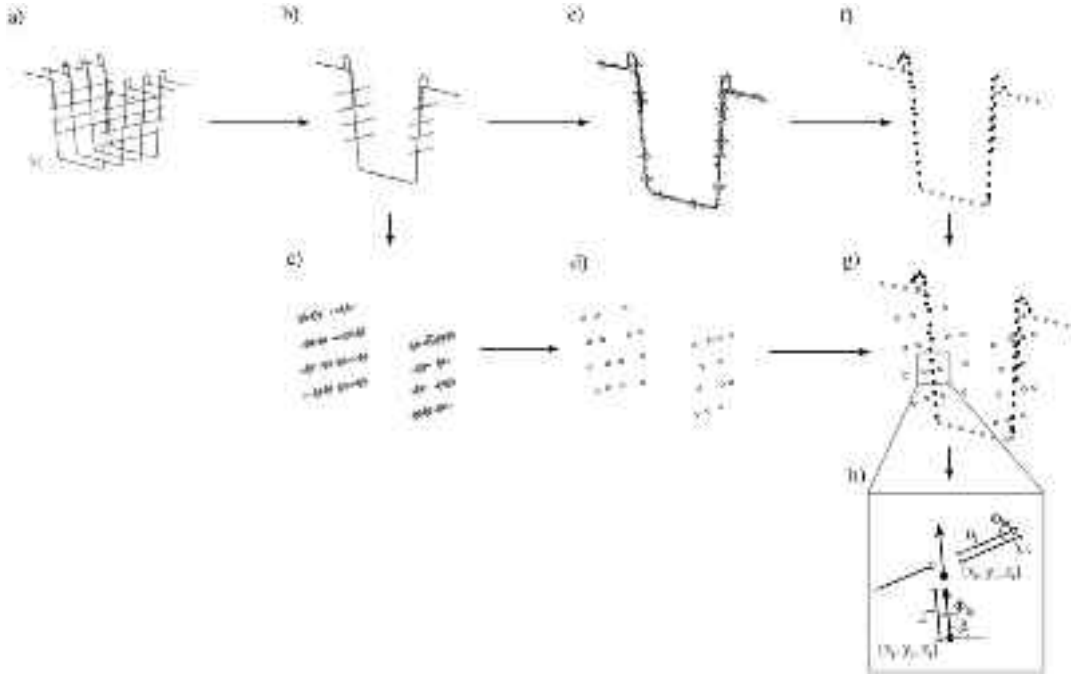

Fig. 5. Method A: a) point cloud, b) point cloud segment, c) circle fitting - longitudinal rebar, d) longitudinal rebar data, e) circle fitting - vertical and horizontal rebar*, f) vertical and horizontal rebar points*, g) combined rebar points, and h) rebar points showing associated output data. (* Longitudinal rebar omitted for clarity in these sub-figures).

The cleaned point cloud is translated to a new axially-aligned Cartesian reference frame as shown in Fig. 5b, with global 3D origin (0,0,0) located at the centre of the point cloud. The x, y and z axis orientations are identified from fitted bounding boxes in each of the xy, yz and xz planes.

3.2.2. *Rebar set region detection*

A recursive slicing method is developed to segment an oriented point cloud into individual rebar set regions, Fig. 5a-b, where each region contains both longitudinal rebar and a single rebar set. Each identified region is then further segmented into either longitudinal rebar, Fig. 5c, or a rebar set consisting of transverse and vertical rebar, Fig. 5e. Slice locations are based on point cloud density patterns that arise from Characteristics 1, 2, and 3 in Section 3.1.

Slice locations for rebar set regions are evaluated from the oriented reinforcement cage PCD, shown in plan (xy) in Fig. 6a. Bar set locations can be observed as high density regions that extend the full width of the cage, rotated at an arbitrary angle to the transverse y axis. These high density regions are separated by low density regions that correspond to longitudinal rebar locations. A 2D density distribution is evaluated over a coarse 20 × 40 mm cell grid in the xy plane, Fig. 6b, with the density histogram from the central row (y = 0) plotted in Fig. 6c. The minimum cell grid size is based on a minimum cover requirement of 15 mm for DTMR concrete elements plus half the minimum rebar diameter of 10 mm [17,49]; the maximum cell grid size is based on maximum rebar diameter of 40 mm.

In measuring from left-to-right, a grid cell can be identified for the start of each rebar set, at locations of increasing density (grey circle). Similarly, in measuring from right-to-left, a cell can be identified for the end of each rebar set (hollow black square). Additional point pairs can be evaluated along grid rows to either side of the central row, Fig. 6b, to give six boundary points for each rebar set; a line of best fit through

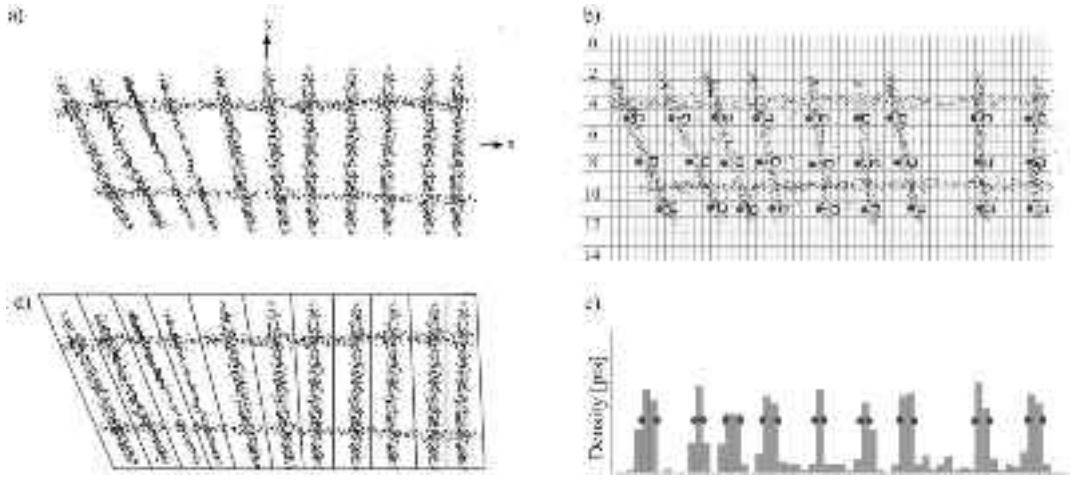

Fig. 6. 2D (xy plane) density distribution for segment identification: a) aligned point cloud, b) grid showing locations of increasing density, c) density histogram along row 8, and d) segmented point cloud.

these six points gives centre location and orientation angle of that particular bar set. Rebar set regions are segmented at the median distance and orientation of neighbouring sets, Fig. 6d.

Segments corresponding to longitudinal rebar and rebar sets can now be determined from individual bar set regions. An example segmented region is shown in Fig. 7a, with a local x_i'-y_i' coordinate system defined from the region's identified centre location and orientation angle. A 1D density distribution can be evaluated along the x_i' axis, with a $\Delta x_i' = 10mm$ step size, generating a minimum of one slice per rebar (10 mm minimum rebar diameter, Characteristic 4, Section 3.1). Rebar sets correspond to density peaks bounded by cells with $\gamma \geq 0.75\overline{\gamma}$. Longitudinal rebar corresponds to density troughs, Fig. 7b-c, cells where $\gamma < 0.75\overline{\gamma}$. For each trough identified, a longitudinal segment is extracted from the bar set region, with a length equal to 35% of the trough length; minimising the inclusion of points from any adjacent peak. The longitudinal rebar is present in each segment peak regardless of peak width (Characteristic 3, Section 3.1); the bar set segment corresponds to the entire bar set region.Where no peak or trough is identified, no corresponding longitudinal segment or bar set segment is assigned.

3.2.3. Longitudinal rebar id

As shown in Fig. 5c-f, the longitudinal regions and rebar set regions of each segment are isolated to allow for bar identification. Identification produces a discretised representation of the point cloud, whereby rebar point groups are each assigned a base point in the global axis (x_i, y_i, z_i), length (L_i), orientation (θ_i), and diameter (ϕ_i), per Fig. 5g-h. No prior information regarding these parameters is known, with assigned diameter constrained only by valid rebar diameters, Characteristic 4, Section 3.1. Longitudinal, vertical, and transverse rebar remain as separate groups of rebar points. This section first considers longitudinal bar identification.

Each longitudinal region is first sliced at $\Delta x = 20mm$ increments, to produce longitudinal bar cross sections in the yz plane, Fig. 8a. A 20 mm slice size was adopted based on the concrete cover and rebar diameter, as per Section 3.2.2. Point groups are formed within this slice using a DBSCAN clustering algorithm. Points within a specified maximum distance are grouped together, with any point exceeding the maximum distance of an existing group placed in a new group. Point groups are either retained or discarded based on a specified minimum group size criteria; any group with fewer than the required minimum number of points is considered to be invalid and discarded, Fig. 8d. Threshold parameters for the DBSCAN are 110 mm for the maximum distance and 30 points for the group size. The maximum distance was based on a ϕ_{max} of 40 mm, typical maximum bundle of two bars, a placement tolerance of ±10 mm per rebar [15], and an additional allowance of 10% to account for the slice width and other variations including scan accuracy and rebar ribbing. The minimum group size assumes a lower bound scan resolution of 3.15 mm @ 10 m; based on an average offset of the LiDAR scanner from the reinforcement cage of 4 m (refer Section 4 for further details), a 20 mm slice of point cloud, and a 10 mm minimum rebar diameter.

The centre coordinates and diameter of rebar cross sections are identified from the point groups. A maximum and minimum possible number of cross sections are identified for each point group by dividing the maximum dimension of the group by 10 mm and 40 mm (minimum and maximum rebar diameters) respectively, as shown in Fig. 8e-f, (Characteristic 4, Section 3.1). For each possible division, one or multiple cross sections are generated from a circle fitting algorithm with corresponding diameter, centre location, and fitting error. Overlapping and invalid diameters are excluded to obtain final rebar cross sections, Fig. 8g. A collection of rebar points is created for the longitudinal region, where each rebar point corresponds to a cross section with the minimum fitting error for a point group, Fig. 5h. The diameter and centre coordinates of the fitted cross section are associated with the rebar point.

The rebar points are combined into individual rebar to generate output data as bar orientation and length. Rebar points are grouped based on the distance between their centres in the yz plane; rebar points not exceeding the proximity requirements of $|O_i - O_j| < \overline{\phi}_{ij}$ are grouped, rebar points exceeding this maximum distance when compared against all other groups are placed in a new group. Using the third characteristic in Section 3.1, each longitudinal rebar must be present in the longitudinal region of multiple segments, therefore groups with a size less than 50% of the number of troughs are discarded. As each group is considered to be a single rebar, the diameter associated to each cross section is updated to equal the mode of the diameters for the group. Following grouping, the length and orientation of each rebar point can be calculated using the adjacent rebar points.

3.2.4. Vertical/transverse rebar id and output

Bar set regions are processed in a similar manner as above to extract vertical and transverse rebar attributes, Fig. 5f-g. This is conducted in two separate stages, creating two sets of point groups which are stored and further processed individually. Segments are first sliced at $\Delta z = 20mm$ increments, to produce vertical bar point groups in the xy plane, Fig. 8b. Segments are separately sliced at $\Delta y = 20mm$ increments to produce transverse bar cross-sections in the xz plane, Fig. 8c. Cross sections are identified with the DBSCAN and circle-fitting algorithm as described above, using the same distance, size, and minimum fitting error criteria.

The bar set region contains points corresponding to longitudinal rebar, thus any cross sections incorrectly identified from these points must be removed. Vertical and transverse rebar cannot exist at the same location as longitudinal rebar, therefore cross sections where $|O_v - O_l| < \overline{\phi}_{vl}$ or $|O_t - O_l| < \overline{\phi}_{tl}$ are discarded. Following the removal of invalid cross sections, the rebar points with associated data (Fig. 5h) can be generated, with x, y, z coordinates and ϕ obtained from the circle fitting algorithm, L obtained from the slice size, and θ obtained from a line of best fit through each point group.

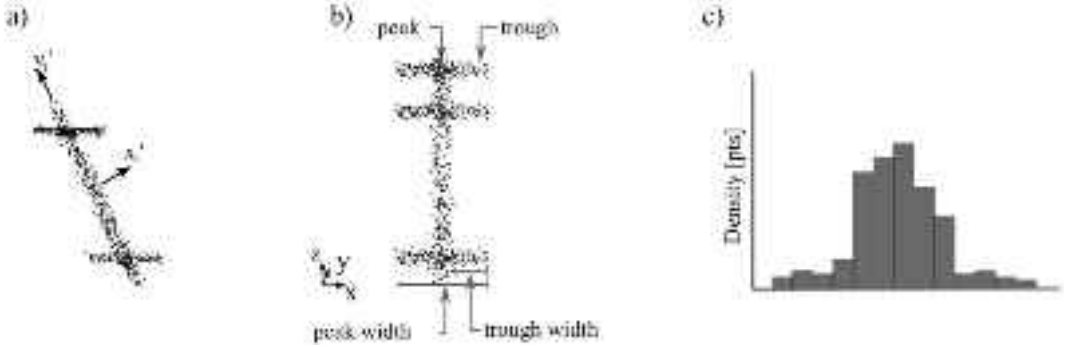

Fig. 7. Segment orientation and alignment: a) point cloud segment, b) Elevation - aligned segment along global x-axis, and c) 1D density histogram along x-axis.

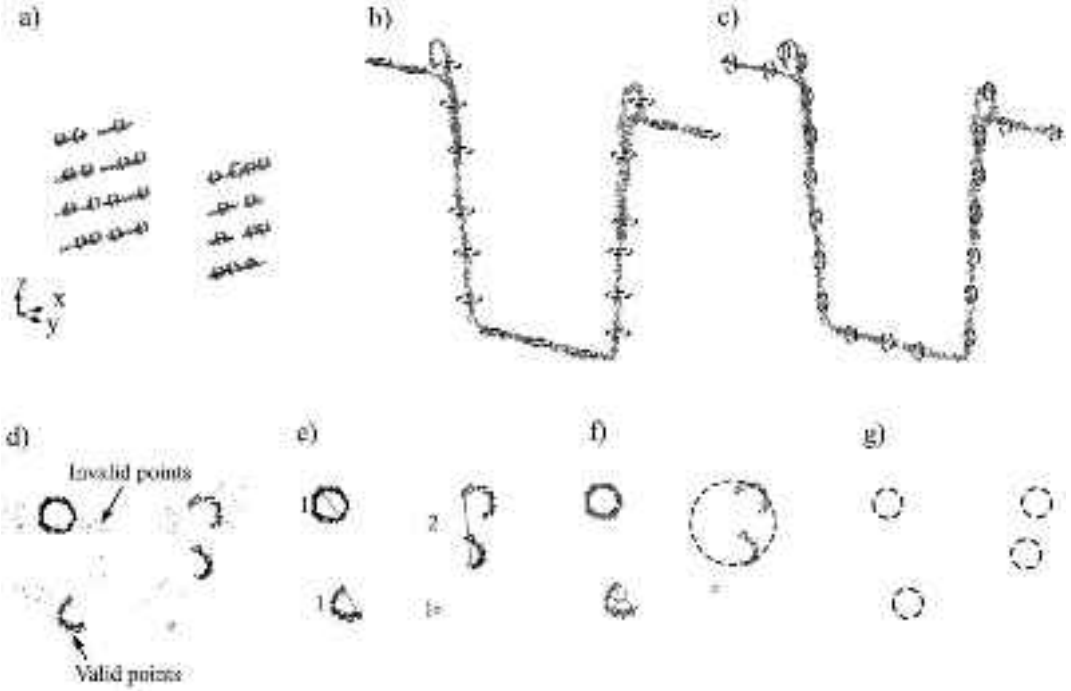

Fig. 8. Grouping and circle fitting for a) longitudinal, b) vertical*, and c) horizontal* rebar in yz, xy and xz planes, respectively. Rebar identification steps: d) DBSCAN grouping, e) bundled bar identification, f) minimum error circle fitting, and g) circle of best fit. *Longitudinal rebar omitted for clarity.

3.3. Semantic enrichment method - bottom up grouping for Bar shape reconstruction

The second processing method generates semantic information related to the reinforcement cage, including rebar shapes, quantities, and total length, using outputs received from the above slicing method. The bar shape grouping established by this processing method is also expected to improve consistency and accuracy of rebar identification [35], ensuring a consistent diameter for rebar segments associated to an individual rebar shape. The workflow comprises three stages as shown in Fig. 9b-d: a knowledge-based grouping of discretised rebar points, bar shape identification based on rebar group bend characteristics; and reconstruction and output of individual bar geometries. Semantic enrichment parameters utilise the nomenclature presented in Section 3.2, and additional parameter Euclidean distance d.

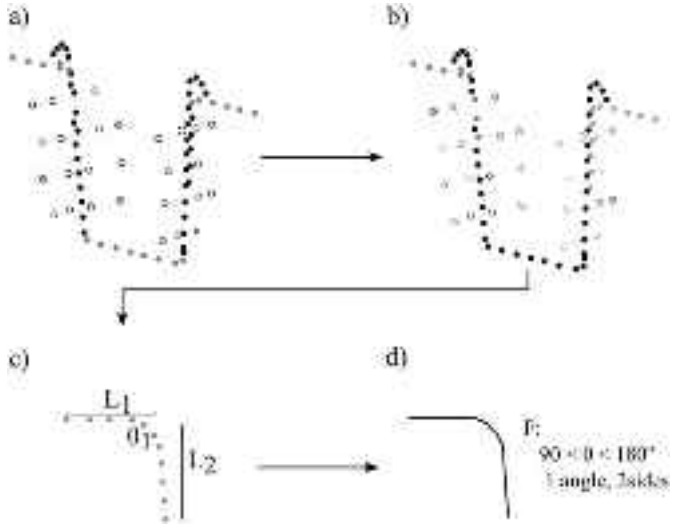

Fig. 9. Method B a) input from Method A, b) individual rebar grouping, c) rebar side and bend identification, and d) rebar shape identification.

3.3.1. Rebar grouping

The sorted vertical and transverse rebar points, output from the slicing method, are combined into their separate rebar using a recursive grouping algorithm. This is implemented in three stages, Fig. 10, with each stage increasing the size and number of rebar points assigned to any particular group through relaxation of permissible tolerances.

The first stage is an initial grouping of vertical and transverse rebar points, based on the proximity of adjacent rebar points. Perpendicular grouping tolerances are based on the minimum cover for DTMR concrete elements, and the minimum rebar diameter. Out-of-plane tolerances (Δx) are based on the segment rebar diameter, with a lower bound of 75% of the minimum rebar diameter to minimise impact from small wires and rebar that may be included for construction purposes. These tolerances are set as: $\Delta z \leq 30$ mm and $\Delta y \leq 50$ mm (2.5 times slice size) for transverse cross sections; $\Delta y \leq 30$ mm and $\Delta z \leq 50$ mm for vertical cross sections; and $\Delta x \leq x_{max}$, where x_{max} is the maximum of 7.5 mm and 0.95ϕ. A limit is placed on Δx to constrain the out-of-plane drift of adjacent points. At the end of this stage, any group containing a single rebar point is discarded.

The second stage creates corner groups by identifying intersecting vertical and transverse groups, based on segment end point proximity and intersection validity. The end points of each vertical group are checked against the end points of all transverse groups to determine the nearest of any valid intersections. An increased tolerance is allowed in this second stage, based on the minimum DTMR spacing of 90 mm [16], and a minimum allowable tolerance of 15 mm [49]. End point grouping tolerances are set as: $d \leq 75$ mm between segment end points (Fig. 11a), and $\Delta x \leq x_{max}$, where x_{max} is:

$$x_{max} = \begin{cases} \dfrac{(\phi_i + \phi_j)}{2}, & \text{if } d \leq 2 \times L \\ 0.3 \times \dfrac{d}{L} \times \dfrac{\phi_i + \phi_j}{2}, & \text{if } d > 2 \times L \end{cases} \quad (1)$$

Δx is thus differentiated based on the distance between adjacent end

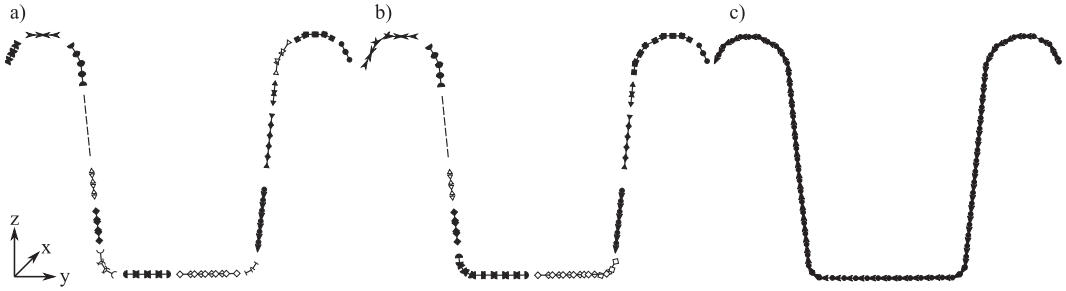

Fig. 10. Grouping stages (groups differentiated by line type) a) Stage 1 - vertical and transverse groups, b) Stage 2 - vertical, transverse and intersection groups, and c) Stage 3 - final groups.

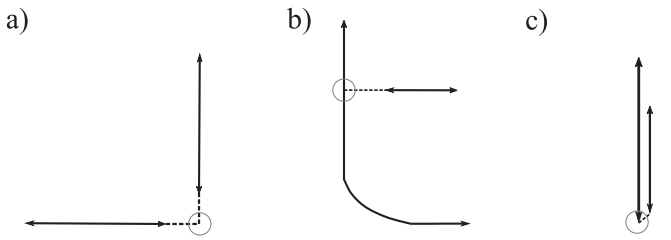

Fig. 11. Invalid group intersections a) maximum distance, b) internal intersection, and c) overlapping segments.

points, allowing larger permissible offsets to be interpolated for segments spaced further apart. Additional constraints are placed on the location of the segment intersections; segments cannot intercept internally within either segment (Fig. 11b) or overlap (Fig. 11c). At the end of this stage, any groups containing two rebar points are discarded.

The third stage recursively joins the identified vertical, transverse, and corner groups together. Each group is compared against all other groups, in ascending order of distance between end points. The grouping requirements from stage 2 are retained, with a relaxation on the maximum distance to: $d \leq 175$ mm. Once the final groups have been formed, any group with $L < 0.25\overline{L}$ is removed.

3.3.2. Rebar shape identification

The grouped rebar points are classified against a known library of rebar shapes (Characteristic 5 Section 3.1). The library used in the algorithm has been created from the DTMR standard bar shapes [18], where each individual rebar shape is uniquely characterised by the number of bends, angle of bends, and number of sides it contains, as shown in Fig. 12.

For each bar group, including the longitudinal rebar grouped in Method A, a centreline of the rebar is created from the sorted rebar points. The number of sides, number of bends, and angle of bends are extracted and compared against the library shapes. The matching bar shape or 'UNKNOWN' is output to the user and associated with the rebar points within the bar group. The diameter of all segments are updated to the mode of the diameters contained in each group.

3.3.3. Post-processing

For final output, the geometric information determined from the slicing method is combined with the bar group and shape information determined from the semantic enrichment method. Additional positional and dimensional parameters as related to reinforcement cage QC are also quantified for final output. Output geometric information includes location and skew angle of rebar sets; and diameter, location, and inclination of rebar points. Output semantic information includes the shape and diameter of bar shape groups, total rebar length, rebar length per diameter (before and after grouping), and bar shape quantities. The outputs of these two methods presented can also generate a semantic 3D model of the reinforcement cage. An example is shown in Fig. 13, generated using 3D parametric CAD software Rhino/Grasshopper.

4. Implementation

For algorithm validation, scan data was collected from two bridge girder reinforcement cages at a local precast yard, shown in Fig. 14a-b. Scanning was conducted with a Leica Scanstation P16, with scan resolution set to 3.1 mm at 10 m. Each full 360^o scan took approximately 3.5 min (excluding set up time) and scans were registered using the Leica Cyclone software. Total time for data collection and analysis was 3.5–5 h, comprising 0.5–1 h to scan, 2 h for scan registration, and 1–2 h to process the point cloud through the algorithm. Scan and reinforcement cage parameters are summarised in Table 2 and Table 3.

'Scan A', shown in Fig. 14c, is a typical 1500 Super T end block reinforcement cage, approximately 2.1 m long, with 17 rebar sets splayed between 0^o - 9.5^o and with two lifting loops. Individual rebar were all N16 (16 mm diameter) with five standard rebar shapes being utilised. Sets were spaced at approximately 150 mm centres and had three layers of rebar. The total point cloud (~5.2 million points) was comprised of four scans taken at different orientations and distance

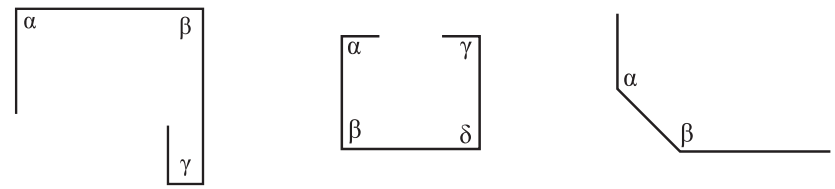

EB:
$\alpha \approx \beta \approx 90^o$
$\gamma \approx 180^o$
2 angles, 1 hook,
4 sides

MD:
$\alpha \approx \beta \approx \gamma \approx \delta \approx 90^o$
4 angles, 5 sides

H:
$\alpha + \beta \approx 90^o$
2 angles, 3 sides

Fig. 12. Example DTMR bar shapes.

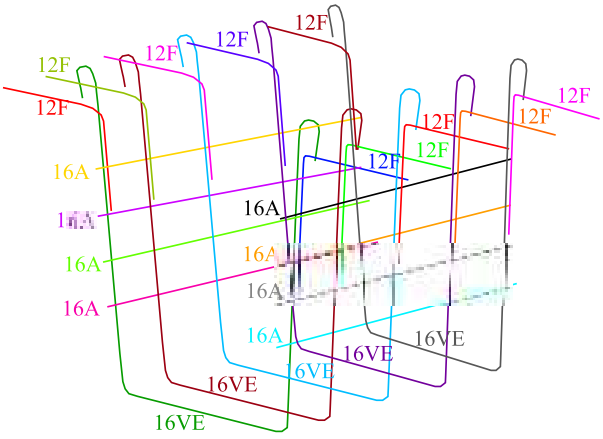

Total Length Rebar [m]	34.75
Length 10mm Rebar [m]	0.00
Length 12mm Rebar [m]	8.25
Length 16mm Rebar [m]	27.25
Length 20mm Rebar [m]	0.00
Bar Shapes and No. Of	8-16A, 10-12F, 5-16VE

Set Skew [°]	2.1, 3.8, 3.2, 4.4, 6.7
Set Centres [m]	-0.25, -0.15, -0.02, 0.13, 0.29

Fig. 13. 3D Model showing generated QC data.

around the cage, as required to work within the constraints of an active site. Scan data was captured whilst raining. For locations of scans, refer Fig. 14e.

'Scan B', Fig. 14d, is a typical 1000 Super T midspan reinforcement cage, approximately 8 m long with rebar sets splayed between 0^o - 4^o and with two lifting bars. Individual rebar were N12 and N16 (12 mm and 16 mm diameter) with three standard rebar shapes being used. The 45 sets of rebar had the same arrangement, with centre spacing between 150 mm and 300 mm, and each set comprised of two layers of rebar. The point cloud (~10 million points) was formed from six scans located at varied distances and orientations to the cage, to suit site constraints. For locations of scans, refer Fig. 14f.

The algorithm presented in Section 3 was implemented in C++, using standard C++ libraries and an open source implementation of the DBSCAN algorithm. The input point cloud data was exported as text files from Leica Cyclone and CloudCompare. The code was run on a Windows 10 laptop with 8GB RAM, Intel i7 1.80GHz processor and data read from and written to an external 3.0 USB HDD.

The algorithm outputs for Scan A and Scan B point clouds are summarised below, with comparison against as-built values. For Scan B the point cloud size was randomly reduced by 50%, to ~5 million points, approximately the same density (by rebar length) as Scan A. The lifting loops and bars shown in Fig. 14a and Fig. 14b were excluded from both the algorithm and as-built results.

5. Results

5.1. Rebar arrangement

Rebar sets identified by the algorithm are shown in Fig. 15, overlaid on the raw point cloud of Scan A and Scan B. The number of sets was determined correctly for both scans. Set orientation, as measured by splay angle along the centre of the rebar set, is compared against as-built values in Fig. 16a. Splay angles had a median difference of 0.5^o and 0.1^o for Scan A and Scan B respectively, and with a maximum difference of 2.1^o and 1.2^o. Set spacing, as measured from centre points, is compared against as-built values in Fig. 16b. Set spacing had a median difference of 1.7 mm and 0.7 mm, and maximum difference of 18.3 mm and 20.4 mm for Scan A and Scan B, respectively. Manual measurement of the PCD in Rhinoceros was used to determine as-built measurements. Skew and spacing values for all bars sets are tabulated in Supplementary Material SP1, Tables 1 and 2.

5.2. Rebar quantity

The measured values for total length of rebar and length of rebar by diameter are shown in Fig. 17 and Table 4. Rebar quantities are reported from two stages of the algorithm: 'ungrouped' results in Fig. 17a-b are output after the initial slicing method (Method 1), and 'grouped' results in Fig. 17c-d are output after the subsequent semantic enrichment method (Method 2). As-built rebar lengths were obtained from manual tracing of the centreline of the point cloud in Rhinoceros and as-built rebar diameters were based on available design information [16] and confirmed with the precast yard. Total length values for all bar sets are tabulated in Supplementary Material SP1, Table 3.

For longitudinal rebar total lengths, the absolute difference ΔL between ungrouped algorithm measurements and as-built values was 0.41 m and 7.76 m for Scan A and Scan B, respectively. For grouped algorithm measurements, this improved to an absolute difference of 0.07 m and 0.13 m for Scan A and Scan B, respectively. From the total length L of longitudinal reinforcement as listed in Table 3, measurement accuracy is evaluated as (L - Δ L) / L. Ungrouped length accuracy is 94% and 88% for Scan A and Scan B, respectively, improving to 99% and 100% for grouped length accuracy.

From the as-built measurements of bar sets as listed in Table 3, individual bar sets in Scan A and B have lengths of 19.38–19.68 m and 5.05 m, respectively. By comparison, algorithm measurements had an average absolute difference and accuracy (bracketed) for ungrouped measurements of 1.32 m (93%) and 0.47 m (91%) for Scan A and Scan B, respectively, with a maximum difference (minimum accuracy) of 3.96 m (80%) and 1.99 m (61%). For grouped algorithm measurements, average absolute difference was 1.89 m (90%) and 0.07 m (99%) for Scan A and Scan B, respectively, with a maximum difference of 5.05 m (74%) and 1.91 m (62%).

Algorithm measurements as differentiated based on rebar diameter are listed in Table 4. Scan A had a total as-built length of 16 mm bar of 341.0 m; ungrouped algorithm measurement for this identified diameter had an absolute difference and accuracy (bracketed) of 250.1 m (27%), improving to 119.4 (65%) with grouping. Scan B had total as-built lengths for 16 mm and 12 mm bar of 208.1 m and 83.3 m, respectively. The absolute difference of ungrouped and grouped measurements was 47.4 m (77%) and 9.2 m (96%) for 16 mm bar, and 48.5 m (42%) and 57.2 m (31%) for 12 mm bar.

5.3. Individual rebar and Bar shapes

Individual rebar groupings and identified shapes for Scan A and B are listed in Supplementary Material SP1 Section 1.3. The accuracy of these results have been assessed in two stages: the number of rebar detected compared to the as-built number of rebar, and the correctness of the identified rebar shapes. Table 5 summarises the number of identified individual rebar for Scan A, compared against that identified manually from the point cloud.

Rebar groups have been assessed as 'correct', 'partial' or 'incorrect',

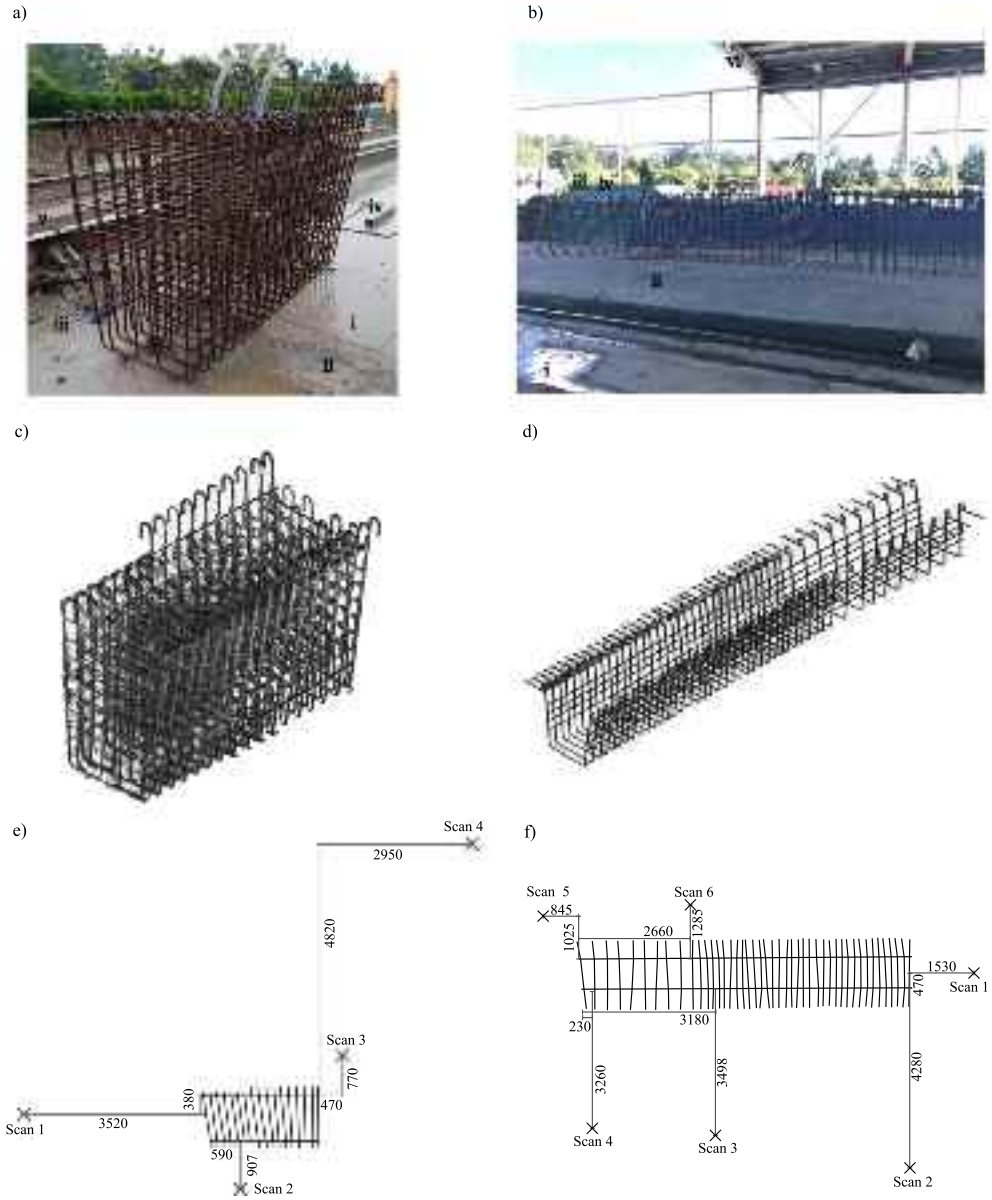

Fig. 14. Scan A and Scan B reinforcement cages, a) Scan A photo, b) Scan B photo, c) Scan A point cloud, d) Scan B point cloud, e) Scan A LiDAR scan locations ('X') and distance from cage, and f) Scan B LiDAR scan locations ('X') and distance from cage. For a and b, site considerations include: i) puddles, ii) uneven ground, iii) limited space, iv) surrounding objects, v) adjacent casting pit, and vi) varied lighting conditions.

Table 2
Scan information.

Scan	Scan A	Scan B
Number individual scans	4	6
Scan resolution	3.15 mm @ 10 m	3.15 mm @ 10 m
Total time [min]	300	210
Registration error [m]	0.001	0.002

Table 3
Reinforcement cage information, including number of bars (no.) and total length (L).

Scan	Scan A		Scan B	
	No.	L [m]	No.	L [m]
Longitudinal rebars	4	8.6	8	64.1
Rebar sets	17	332.5	45	227.3
Total rebar (individual bars)	174	341.0	143	291.3
Rebar Diameters [mm]	16	341.0	16	208.1
			12	83.3

as shown in Fig. 18. Correct rebar groups, are those where the grouped segments correspond to the actual as-built rebar (such as Fig. 18a and d). Partial rebar groups refer to grouped subsegments of the actual rebar shape, for example the vertical leg of bar i and the right hand portion of bar ii in Fig. 18b; or the inclined and horizontal portion of bars iii and iv in Fig. 18e. Rebar groups which do not fall into either category, grouping segments of different actual rebar, are classified as incorrect, Fig. 18c, and f. For Scan A, no rebar groups formed contained a correct rebar, and 25% of groups contained a valid partial rebar. For Scan B, 21% of rebar points were correctly grouped, and 28% of groups contained a valid portion of a single rebar.

Table 6 summarises the number of correct and incorrect rebar shape results returned by the algorithm for Scan A and Scan B. The correct bar shapes have been determined manually by comparing the point cloud and photos of the rebar cages to the DTMR Standard Bar shapes shown

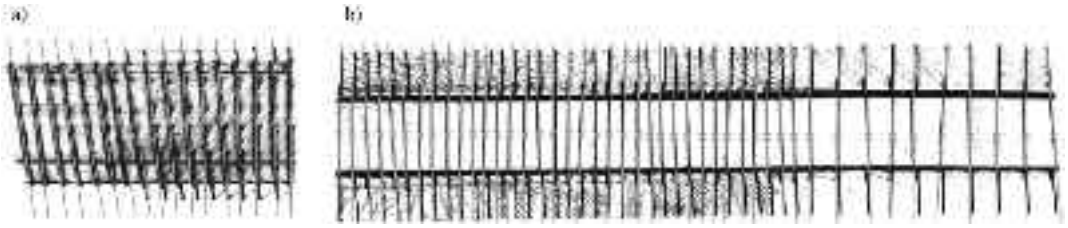

Fig. 15. Raw point cloud versus algorithm orientation for a) Scan A and b) Scan B. Grey lines are inclined to the angle determined by the algorithm and the centre of the rebar set is located at the 'X'.

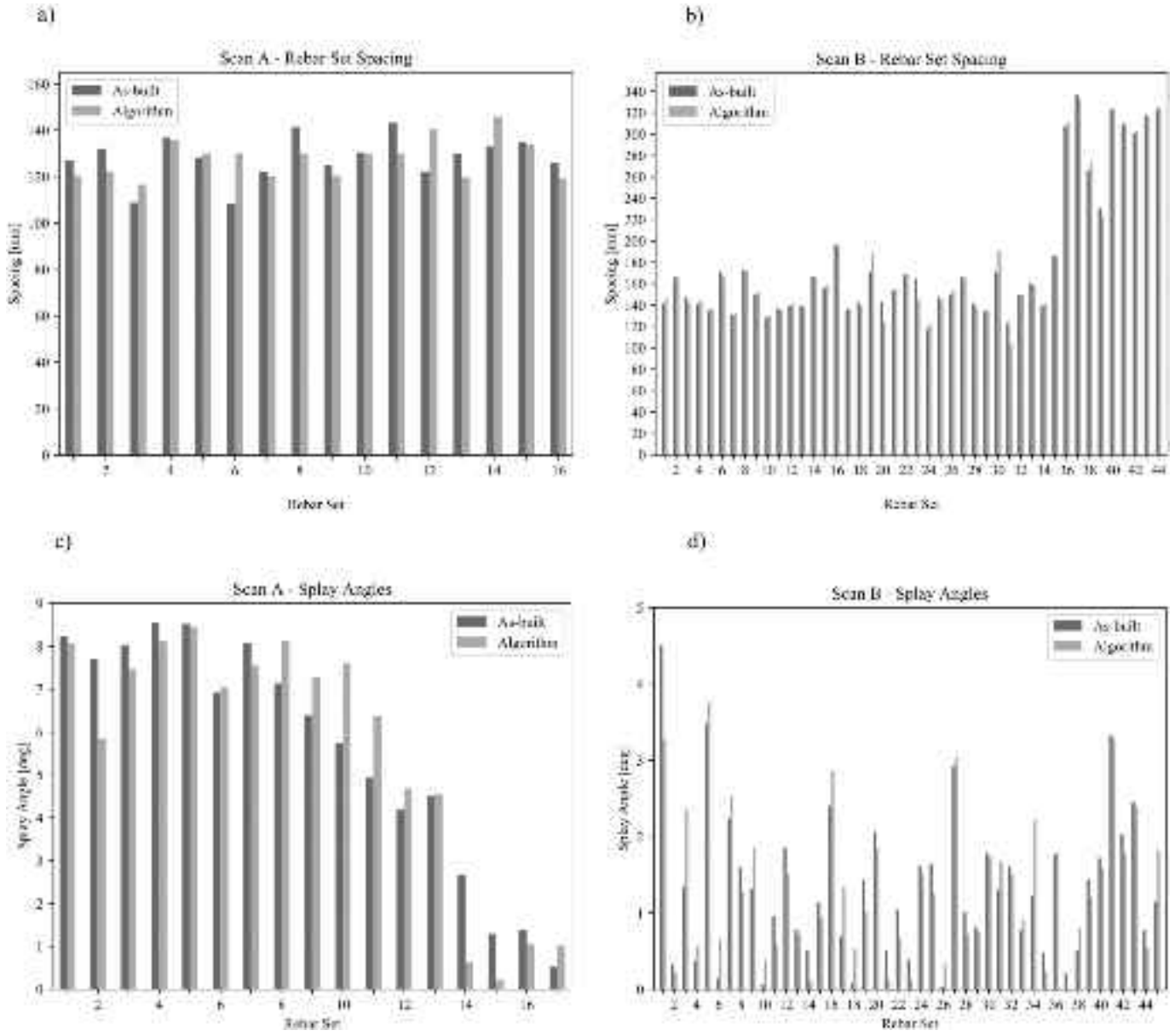

Fig. 16. Set spacing and splay angle a) Scan A spacing, b) Scan B spacing, c) Scan A splay angles, and d) Scan B splay angles.

on standard drawings [18]. The straight longitudinal bars are all correctly identified for both Scan A and Scan B. The shape of the individual rebar within the sets is identified with an accuracy of 20% and 30% for Scan A and Scan B respectively.

5.4. Summary

Several key geometric measures of bridge girder reinforcement cages were automatically extracted from acquired point clouds. As identified in Section 2.2, these measures can be utilised in assessing compliance to QC requirements. Positional QC variables including the rebar spacing and skew (Section 5.1) and dimensionsal QC quantities such as the total

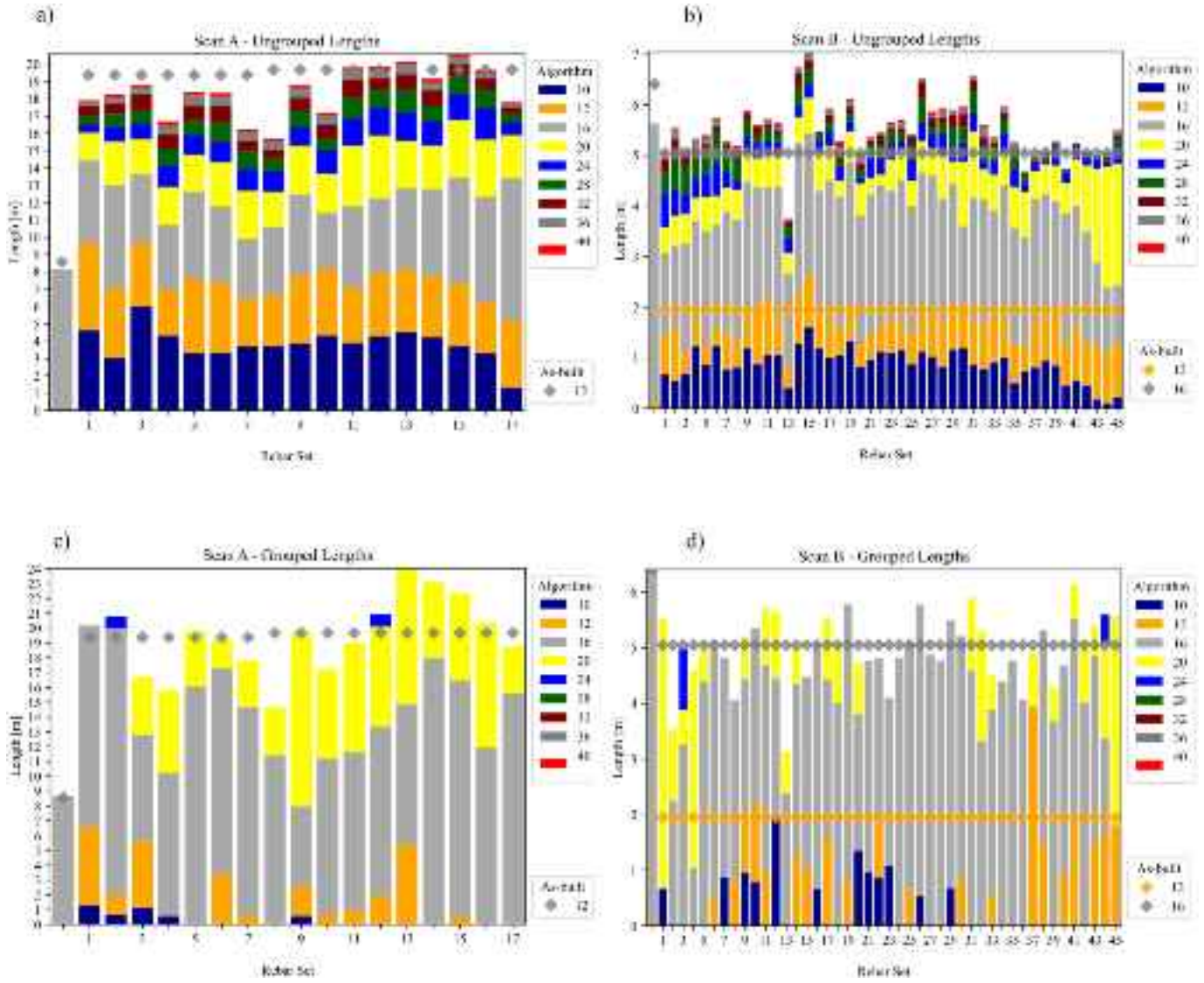

Fig. 17. Rebar length by diameter a) Scan A ungrouped, b) Scan B ungrouped, c) Scan A grouped, and d) Scan B grouped. Set 0 refers to longitudinal rebar. Scan B longitudinal rebar length scaled by a factor of 1/10.

Table 4
Rebar length by location (top) or by diameter (bottom) [m].

	Scan A		Scan B	
Location/Diameter	Ungrouped	Grouped	Ungrouped	Grouped
Longitudinal	8.17	8.65	56.32	63.95
Average Bar Set	18.4	19.44	5.51	4.98
10	65.5	4.2	39.4	11.4
12	61.6	26.5	34.8	26.0
16	90.6	221.6	160.7	217.3
20	44.24	85.2	33.8	31.6
> 20	59.6	1.7	13.4	1.6

length of rebar and total length of different rebar sizes (Section 5.2) were quantitified. Application of the semantic enrichment method (Sections 5.2 and 5.3) resulted in a higher accuracy of quantities reported. Additional data for QC verification could also be determined, including the number of individual rebar present and their corresponding shape.

Table 5
Number of individual rebar.

	Scan A		Scan B	
	Longitudinal rebar	Rebar sets	Longitudinal rebar	Rebar sets
Total rebar detected [−]	4	210	8	142
Total as-built rebar [−]	4	170	8	135
Correct rebar [−]	4	0	8	30
Partial rebar [−]	0	42	0	40
Incorrect rebar [−]	0	168	0	72

6. Discussion

6.1. Algorithm efficacy

As demonstrated by the results presented in Section 5, a decrease in the algorithms' efficacy, compared to the as-built dimensions, occurred with increasing complexity in the inference of the knowledge-based

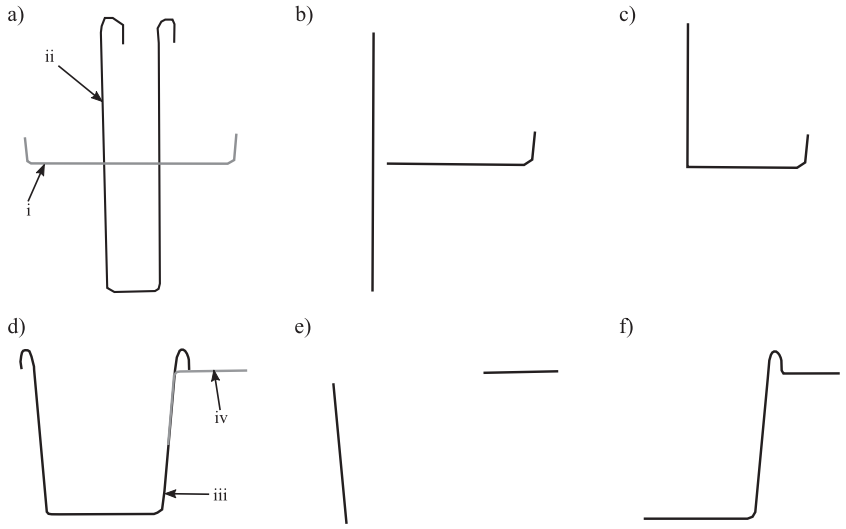

Fig. 18. Grouping examples, a) Scan A correct groups, b) Scan A partial groups, c) Scan A incorrect groups, d) Scan B correct groups, e) Scan B partial groups, and f) Scan B incorrect groups.

Table 6
Rebar shape identification.

	Scan A		Scan B	
	Longitudinal rebar	Rebar sets	Longitudinal rebar	Rebar sets
Correct rebar shape[a] [−]	4	41	8	43
Incorrect rebar shape [−]	0	169	0	99

[a] Incorrectly grouped rebar which are assigned the correct shape for the resultant group shape are counted as correct.

rules. The rebar set spacing and skew had an average error of approximately 6.3% (Scan A) and 2.7% (Scan B) for spacing and average skew error of less than 0.1^o (Scan A and B). Reported errors in measured spacings of rebar in slab type arrangements ranged between 0.5% to 6.3% [34,35,57,59]. Currently, no study has been found quantifying the skew and measurement error for sets of multiple rebar identified in point clouds.

The total length of rebar reported by the algorithm had an average accuracy of 94% and 99% for the ungrouped and grouped results respectively. The length of rebar by rebar diameter demonstrated a similar relationship between ungrouped and grouped results, with average accuracies of 45% and 70%. The improved accuracy of rebar diameter identification was also reported by [35], with accuracy increasing from 55.2% to 72.7% at 0.036^o resolution. It was noted that the results for Scan A include one outlier, set 8, in terms of detected length; with this having one of the lowest point densities and the greatest occlusion. When the results from this set are excluded, accuracy of average ungrouped length per set increases from 93% to 94%, and once grouped from 90% to 92%; similar to the improvements reported by Scan B.

The longitudinal, straight, rebar were correctly grouped into each individual rebar, while for rebar within sets approximately 10% were correctly grouped and 26% of rebar groups partially formed. No study has been identified reporting results of grouping non-straight rebar. For shape identification, an overall accuracy of approximately 25% was reported. The tolerance and accuracy of the identified bend angles was identified as common source of error in bar shape identification; the outer rebar in both Scan A and Scan B is inclined at a theoretical 95.4^o. Identified bend angles varied between approximately 82^o and 100^o, corresponding to three base rebar shapes 'D' (90^o), 'F' ($>90^o$), and 'G'($<90^o$) for two sided rebar and seven base rebar shapes for three sided rebar. The results of the bar shape identification are unable to be benchmarked as, to the authors' knowledge, the algorithms presented are the first to identify rebar shape information from geometric point cloud data.

The geometrical measurement accuracy of the algorithm is lower than comparable measures from other studies. Factors identified as potential contributors include: increased occlusion and noise within the rebar cage due to the increased density, multiple layers of rebar in all axes (as identified by [34]), and the effects of scanning in on-site (similarly reported by [31,32]).

The developed methodology has been based and tested on bridge girders, utilising identifiable characteristics of reinforcement. The key characteristic used within both methods, the distinct division between longitudinal, vertical, and transverse rebar, is shared by reinforcement for many RC archetypes, including bridge headstocks, slabs, piles, and beams. The list of key characteristics (Section 3.1), could be adapted to include other criteria to suit helix reinforcement (such as in piles), penetrations within RC elements and reinforcement cages (such as in slabs), or corbels (such as in beams and slabs). The commonality of this key characteristic between reinforcement cages would allow for the adaptation of the methodologies, or the development of a generalised implementation, applicable to a broader scope of elements.

6.2. *Application for QC*

Regarding the algorithm efficacy for QC, the tolerances adhered to by industry have been adopted for comparison to the algorithm output. Positional QC measures discussed in Section 2.2, allow a tolerance on rebar spacing equating to 15 mm for Scan A and 18.2 mm for Scan B; while for skew the permissible tolerance is 48 mm over the 800 mm base width, equivalent to 3.4^o. From the results obtained, Scan A has 15 spacing measurements within the tolerance (94%), and 40 within the tolerance (90%) for Scan B. All skew measurements for Scan A and Scan B were within required tolerances. The locations in Scan B exceeding the spacing tolerance correspond to locations with lifting bars installed, the effect of the lifting bars on these regions of the point cloud (occlusion and noise) may contribute to the lower accuracy reported. Similarly for Scan A, the sets exceeding the tolerance were adjacent to lifting hoops and showed the greatest degradation of point cloud quality.

For dimensional QC, the total rebar length was within 2 m and 3.5 m for Scan A and Scan B. This equates to an average measurement error of between 11 mm and 23 mm, per individual rebar, compared to the QC

tolerance of ±5 mm per rebar.

In terms of manual measurement, using a standard tape measure a maximum accuracy of ±1 mm could theoretically be obtained. For spacing and skew, additional differences in measurement can be expected to occur based on the location of measurement, as shown by the variation in the set location and orientation in Fig. 15. At minimum, a similar discrepancy in manual measurement would be likely for the length of bent rebar due to the need to measure consistently along bends. Unlike an algorithmic approach, the variation in manual measurement also contributes to a decrease in the repeatability and objectivity of the measurements.

Information on the number of individual rebar and identification of rebar shape is also used for verification of reinforcement cage QC compliance (Section 2.2). The results obtained suggest that further work is required before sufficient accuracy can be obtained for the QC verification of complex rebar shapes.

6.3. Comparison to current industry practice

Regarding the application of the proposed methodology to industry, four key measures are discussed: time, coverage, accuracy, and cost. As discussed in Section 4, a total time of 3.5–5 h was required for data collection, pre-processing, and algorithm run-time. Manual inspection of the reinforcement cage is reported to be similar to the time required to obtain the scan (0.5–1 h), relying on inspectors with extensive experience overseeing fabrication. Documents published by asset owners and technical institutes [14,22] include the following items for visual inspection: shape, size, position, and rebar documentation. However, the coverage of this visual inspection does not encompass measurement of each rebar length, bend radius and angle, rebar location or multiple measurements of spacing and skew. Table 7, compares the outcomes of the algorithmic inspection to manual inspection based on measures adopted by [1,35].

Potential modifications to the process to increase its viability include reducing time and cost, using data for secondary outputs, and implementing a hybrid manual-algorithmic approach. Reductions in time could be achieved through the use of fixed in-situ LiDAR scanners, removing the requirement to travel to site to obtain the scans, and reducing the time and manual work required for scan registration (saving ~ 2 h). In terms of cost, an initial up-front cost is required to obtain the technology; long-term reductions in the cost per scan may be achieved through reduced or removed travel time for inspection, re-use of technology, and reduced labour time for assessing results. Benefits from the automated generation of a 3D as-built model of the reinforcement cage may contribute to the return on investment, including reduced time and cost to generate as-built data, and increased accuracy of as-built documentation. Additionally, an accurate 3D model of reinforcing has been demonstrated to aid in safe drilling of cast concrete elements, identifying locations where required drill depths will not clash with reinforcement by [23]. Based on the observed strengths and weaknesses of algorithm and manual approach, a hybrid approach to inspection is recommended which can combine prior knowledge regarding the reinforcement cage, such as the diameter and shape of manufactured reinforcement used, in combination with automated determination of spacing, skew, length, and bar locations. This could provide opportunity to increase the comprehensiveness of manual inspection whilst maintaining an acceptable level of accuracy.

6.4. Future improvement

Four areas are identified for further development to improve the proposed algorithms: robust noise removal, improved inference in regions of low density, alternate methods of rebar shape classification, and improved run-time. Areas where noise was not fully removed during the post-processing stages of the Slicing Method correlate to the locations where additional rebar segments were identified, such as where lifting loops were installed. Additionally, points capturing non-rebar items, including lifting loops and bars, are required to be manually removed from the point cloud prior to processing. Removal of this noise from the point cloud during initial preprocessing would reduce error caused by these false positives and decrease the subsequent processing run-time.

Conversely, the presence of incomplete or low density regions of the point clouds was also identified as an error source; resulting in missing rebar quantities and incorrect rebar shapes. Fuzzy logic or machine learning algorithms are likely to be better suited to the additional inference required by the algorithm in these areas. Implementation of machine learning techniques for object classification are likely to improve to the shape identification stages of the semantic enrichment algorithm. Machine learning and fuzzy logic algorithms have been identified as potential methods to increase the accuracy of point cloud processing algorithms for QC [33]. A future machine learning implementation could be developed utilising the output of the presented algorithm as automatically-generated labelled training data, reducing the time and required user-input for development.

Circle fitting algorithms have been identified as a potential source of error for determining rebar diameter [35] with different diameters able to be obtained from different algorithms. The Hyper algorithm was identified as the most suitable for circle identification by [4], and has been implemented in the presented methodology. Despite the benefits of this approach, the registration error of approximately 2 mm, a 2 mm - 4 mm step between rebar sizes, and up to 12% variation in rebar diameter due to ribbing and manufacturing tolerances, are all likely to impact the efficacy of circle fitting for rebar diameter measurement. The development of more robust circle fitting methodologies, or use of a hybrid QC method with input of known bar diameters, would likely benefit the accurate identification of rebar diameters.

Table 7
Inspection considerations.

Scan	Inspection Method	Average Time [min]	Inspection Item	Coverage [%]	Accuracy [%]	In-tolerance
Scan A	Algorithm	210	Spacing	100	94	15 of 17
			Skew	100	100	17 of 17
			Total length	100	99	0 of 1
			Diameter	98	65	N/A
			Shape	98	21	N/A
	Manual [35]	99[1]	Set spacing, diameter	100	100	N/A
	Manual [1]	52[1]	Number rebar, spacing	100	70	N/A
Scan B	Algorithm	300	Spacing	100	90	40 of 45
			Skew	100	100	45 of 45
			Total length	100	99	0 of 1
			Diameter	98	77	N/A
			Shape	98	34	N/A
	Manual [35]	105[1]	Set spacing, diameter	100	100	N/A
	Manual [1]	43[1]	Number rebar, spacing	100	70	N/A

[1] Inspection time scaled based on number of rebar and number of sets.

Discussions with the precast yard indicate that an automated platform, for processing reinforcement cage point clouds, would be required to have a run-time equal to, or faster than, the current manual inspection duration, requiring near real-time scanning and processing. The run-time presented in Section 4 does not meet this requirement, although cloud computing implementations may allow for readily accessible, near real-time implementations. Additionally, reducing the quantity of redundant points processed and improved shape recognition are expected to aid in reducing run-time.

7. Conclusion

This paper presents an automated methodology for quantifying geometric and semantic characteristics of bridge girder reinforcement cages, commonly assessed in quality control processes, from utilising LiDAR point cloud data. The implemented algorithm uses a top-down approach to decompose the point cloud, determining the rebar spacing, orientation and creating cylinder-like segments of rebar with a best-fitting centre point, direction, and diameter. A semantic enrichment algorithm is then used to group the cylinders into individual rebar and assign a likely rebar shape.

The proposed methodology was tested on point clouds of two bridge girder reinforcement cages obtained at a precast yard. The geometry of the rebar cage was within a median of 4.3 mm and 0.6^{o} for the spacing and orientation of each set, respectively. A comparison of the results produced by the algorithm and those determined manually show that the quantity and diameter of rebar could be estimated within approximately 99% and 70% accuracy, respectively. The number of individual rebar grouped and correct rebar shape identification were approximately 10% and 25% respectively.

These results suggest that the methodology presented can provide geometrical and some semantic information which can be utilised for reinforcement cage quality control. For QC application in industry, the proposed algorithm is not yet suitable, however a hybrid approach is considered feasible, combining the high coverage and accuracy achievable for rebar position and length by algorithmic methods with the rapid and accurate inspection of rebar diameter and shape through current human based inspection.

The proposed methodology and study has a number of limitations. Further work is required to increase the accuracy of the identification of complex rebar shapes; current results are not yet sufficient for QC applications. The effectiveness of the methodology has also only been assessed for Super T girders, due to site availability; applications to alternative girder types may present challenges not yet considered and future research should consider scan data collected in different production scenarios. The algorithm has been developed based on the requirements of DTMR, and reinforcement cages not conforming to these requirements may require the algorithm to be extended.

Further development towards generalisable methodologies applicable to a wider range of RC elements is considered feasible; utilising the common characteristic of distinct longitudinal, transverse, and vertical rebar present in reinforcement cages for many RC elements.

Declaration of Competing Interest

None.

Acknowledgements

The authors would like to acknowledge ENCO Precast for facilitating site access and reinforcement cage availability for PCD capture.

Appendix A. Supplementary data

Supplementary data to this article can be found online at https://doi.org/10.1016/j.autcon.2022.104334.

References

[1] Ali Abbas, JoonOh Seo, MinKoo Kim, Impact of mobile augmented reality system on cognitive behavior and performance during rebar inspection tasks, J. Comput. Civ. Eng. 34 (6) (2020) 04020050, https://doi.org/10.1061/(ASCE)CP.1943-5487.0000931.

[2] A. Adán, B. Quintana, S.A. Prieto, F. Bosché, An autonomous robotic platform for automatic extraction of detailed semantic models of buildings, Autom. Constr. 109 (2020) 102963, https://doi.org/10.1016/j.autcon.2019.102963. ISSN 0926-5805.

[3] Manu Akula, Robert R. Lipman, Marek Franaszek, Kamel S. Saidi, Geraldine S. Cheok, Vineet R. Kamat, Augmenting BIM with 3D Imaging Data to Control Drilling for Embeds into Reinforced Concrete Bridge Decks, 2012, pp. 1145–1154, https://doi.org/10.1061/9780784412329.115.

[4] Ali Al-Sharadqah, Nikolai Chernov, Error analysis for circle fitting algorithms, Electr. J. Stat. 30 (2009) 886–911, https://doi.org/10.1214/09-EJS419.

[5] American Concrete Institute, Specification for Tolerances for Concrete Construction and Materials (ACI 117–10) and Commentary-Reapproved 2015, American Concrete Institute, 2010. ISBN 978-0-87031-379-0.

[6] Fred Andrews-Phaedonos, Ensuring quality and durability in concrete construction for major infrastructure, in: The 10th Austroads Bridge Conference, Melbourne, Victoria, 2017. URL. https://trid.trb.org/view/1467987.

[7] Austroads, Guide to Bridge Technology, URL, https://austroads.com.au/infrastructure/bridges/guide-to-bridge-technology, 2018. Last accessed: 18/04/2021.

[8] Austroads Incorporated, RoadFacts 2005, Austroads Incorporated, Sydney, Australia, 2005. ISBN 0–85588–719-2.

[9] Robert Benaim, The Design of Prestressed Concrete Bridges: Concepts and Principles, Taylor and Francis, England, 2007. ISBN 0–203–96205-2.

[10] H. Bian, S.E. Chen, W. Liu, Error sources in proccessing lidar based bridge inspection, Int. Arch. Photogramm. Remote. Sens. Spat. Inf. Sci. XLII-2/W7 (2017) 455–459, https://doi.org/10.5194/isprs-archives-XLII-2-W7-455-2017.

[11] British Standards Institute and Comite Europeen de Normalisation, Bs en 13670: 2009 execution of concrete structures, URL, https://www.thenbs.com/PublicationIndex/Documents/Details?DocId=293741, 2009. Last accessed: 14/09/2021.

[12] Gichun Cha, Seunghee Park, Oh. Taekeun, A terrestrial lidar-based detection of shape deformation for maintenance of bridge structures, J. Constr. Eng. Manag. 145 (12) (2019) 04019075, https://doi.org/10.1061/(ASCE)CO.1943-7862.0001701.

[13] Erzhuo Che, Jaehoon Jung, Michael J. Olsen, Object recognition, segmentation, and classification of mobile laser scanning point clouds: A state of the art review, Sensors 19 (4) (2019), https://doi.org/10.3390/s19040810. ISSN 1424-8220.

[14] Concrete Reinforcing Steel Institute, Ctn-m-1-11 field inspection of reinforcing bars, in: Report, Concrete Reinforcing Steel Institute, 2011, p. 2004. URL, http://resources.crsi.org/index.cfm/_api/render/file/?method=inlineandfileID=2A5B3812-EF2A-D159-61469A70F451412D. Last accessed: 03/10/2021.

[15] Department of Transport and Main Roads, Transport and Main Roads Specification MRTS71 Reinforcing Steel, URL, https://www.tmr.qld.gov.au/-/media/busind/techstdpubs/Specifications-and-drawings/Specifications/Superseded-Specifications/2-Bridges-and-Structures/MRTS71/2009_06/MRTS71_Superseded.pdf?la=en, 2017. Last accessed: 19/11/2021.

[16] Department of Transport and Main Roads, Drafting and Design Presentation Standards Volume 3: Structural Drafting Standards Prestressed Concrete Girders, URL, https://www.tmr.qld.gov.au/-/media/busind/techstdpubs/Bridges-marine-and-other-structures/Drafting-and-Design-Presentation-Standards/Volume-3/Current-versions/Volume3Chapter14.pdf?la=en, 2018. Last accessed: 19/11/2021.

[17] Department of Transport and Main Roads, Transport and Main Roads Specification MRTS70 Concrete, URL, https://www.tmr.qld.gov.au/-/media/busind/techstdpubs/Specifications-and-drawings/Specifications/2-Bridges-and-Structures/MRTS70.pdf?la=en, 2018. Last accessed: 13/10/2021.

[18] Department of Transport and Main Roads, SD1043 Reinforcing Steel Standard Bar Shapes Typical Details and Notes, URL, https://www.tmr.qld.gov.au/-/media/busind/techstdpubs/Specifications-and-drawings/Standard-Drawings-Roads/Bridges/SD1043.pdf?la=en, 2018. Last accessed: 19/11/2021.

[19] Department of Transport and Main Roads, Transport and Main Roads Specification MRTS72 Manufacture of Precast Concrete Elements, URL, https://www.tmr.qld.gov.au/-/media/busind/techstdpubs/Specifications-and-drawings/Specifications/2-Bridges-and-Structures/MRTS72.pdf?la=en, 2019. Last accessed: 13/10/2021.

[20] Department of Transport and Main Roads, Design Criteria for Bridges and Other Structures, URL, https://www.tmr.qld.gov.au/-/media/busind/techstdpubs/Bridges-marine-and-other-structures/Bridge-design-and-assessment-criteria-manual/DesignCriteriaforBridgesandOtherStructures.pdf?la=en, 2020. Last accessed: 02/08/2021.

[21] Department of Transport and Main Roads, Standard Drawings Roads Bridges, Marine and Other Structures, 30/11/2020. URL, https://www.tmr.qld.gov.au/business-industry/Technical-standards-publications/Standard-drawings-roads/Bridges-Marine-and-structures, 2020.

[22] Department of Transport and Main Roads, Checklist CAC073M, MRTS70 Concrete (Insitu, Normal Class) Incorporating MRTS71 Reinforcing Steel, URL, https://www.tmr.qld.gov.au/-/media/busind/techstdpubs/Contract/Contract-administration-system/Checklists/CAC073M.docx?la=en, November 2021.

[23] Mani Golparvar-Fard, Behshad Ghadimi, S. Saidi Kamel, S. Cheok Geraldine, Marek Franaszek, R. Lipman Robert, Image-based 3d mapping of rebar location for automated assessment of safe drilling areas prior to placing embedments in concrete bridge decks, Construct. Res. Congress (2012) 960–970. ISSN 9780784412329, https://doi.org/10.1061/9780784412329.097.
[24] E. Hambly, Bridge Deck Behaviour, 2 edition, Chapman and Hall, Australia, 1976. ISBN 0419172602.
[25] G. Hearn, J. Puckett, Ian Friedland, Tom Everett, Kenneth Hurst, G. Romack, George Christian, R. Shepard, T. Thompson, R. Young, Bridge preservation and maintenance in europe and south africa, in: Report FHWA-PL-05-002, US Department of Transport Federal Highway Administration, 2005. URL, http://international.fhwa.dot.gov/pubs/pl05002/pl05002.pdf. Last accessed: 16/08/2021.
[26] N. Hewson, Prestressed Concrete Bridges : Design and Construction, 2 edition, ICE Publishing, London, 2011, https://doi.org/10.1680/pcb.41134.001. ISBN 978–0–7277-4113-4.
[27] S.M. Iman Zolanvari, Debra F. Laefer, Slicing method for curved façade and window extraction from point clouds, ISPRS J. Photogr. Rem. Sens. 119 (2016) 334–346, https://doi.org/10.1016/j.isprsjprs.2016.06.011. ISSN 0924–2716.
[28] Kosei Ishida, Naruo Kano, Kenji Kimoto, Shape recognition with point clouds in rebars, in: J.E.M.H. van Bronswijk, Geer J. Maas, Fans J.M. van Gassel (Eds.), ISG*ISARC2012 Full paper proceedings, Eindhoven, The Netherlands, June 2012, International Association for Automation and Robotics in Construction (IAARC), 2012. ISBN 978–90–386-3410-4.
[29] Sanna Kaasalainen, Anttoni Jaakkola, Mikko Kaasalainen, Anssi Krooks, Antero Kukko, Analysis of incidence angle and distance effects on terrestrial laser scanner intensity: search for correction methods, Remote Sens. 3 (10) (2011) 2207–2221, https://doi.org/10.3390/rs3102207. ISSN 2072-4292.
[30] Alireza G. Kashani, Michael J. Olsen, Christopher E. Parrish, Nicholas Wilson, A review of lidar radiometric processing: from ad hoc intensity correction to rigorous radiometric calibration, Sensors 15 (11) (2015) 28099–28128, https://doi.org/10.3390/s151128099. ISSN 1424-8220.
[31] Min-Koo Kim, Hoon Sohn, Chih-Chen Chang, Automated dimensional quality assessment of precast concrete panels using terrestrial laser scanning, Autom. Constr. 45 (2014) 163–177, https://doi.org/10.1016/j.autcon.2014.05.015. ISSN 0926-5805.
[32] Min-Koo Kim, Qian Wang, Joon-Woo Park, Jack C.P. Cheng, Hoon Sohn, Chih-Chen Chang, Automated dimensional quality assurance of full-scale precast concrete elements using laser scanning and bim, Autom. Constr. 72 (2016) 102–114, https://doi.org/10.1016/j.autcon.2016.08.035. ISSN 0926-5805.
[33] Min-Koo Kim, Qian Wang, Heng Li, Non-contact sensing based geometric quality assessment of buildings and civil structures: a review, Autom. Constr. 100 (2019) 163–179, https://doi.org/10.1016/j.autcon.2019.01.002. ISSN 0926-5805.
[34] Min-Koo Kim, Julian Pratama Putra Thedja, Qian Wang, Automated dimensional quality assessment for formwork and rebar of reinforced concrete components using 3d point cloud data, Autom. Constr. 112 (2020) 103077, https://doi.org/10.1016/j.autcon.2020.103077. ISSN 0926-5805.
[35] Min-Koo Kim, Julian Pratama Putra Thedja, Hung-Lin Chi, Dong-Eun Lee, Automated rebar diameter classification using point cloud data based machine learning, Autom. Constr. 122 (2021) 103476, https://doi.org/10.1016/j.autcon.2020.103476. ISSN 0926-5805.
[36] Wanqiu Liu, Shen-en Chen, Reliability analysis of bridge evaluations based on 3d light detection and ranging data, Struct. Control. Health Monit. 20 (12) (2013) 1397–1409, https://doi.org/10.1002/stc.1533.
[37] Lu Ruodan, Ioannis Brilakis, Campbell R. Middleton, Detection of structural components in point clouds of existing rc bridges, Computer-Aided Civil Infrastruct. Eng. 34 (3) (2019) 191–212, https://doi.org/10.1111/mice.12407.
[38] De-an Luo, Yan-min Wang, Mining wooden pillar features from point cloud, in: 2009 *International Conference on Information Technology and Computer Science* volume 2, 2009, pp. 65–68, https://doi.org/10.1109/ITCS.2009.151.
[39] Josh McCulloch, Richard Green, Extraction of utility poles in lidar scans using cross-sectional slices, in: 2016 International Conference on Image and Vision Computing New Zealand (IVCNZ), 2016, pp. 1–4, https://doi.org/10.1109/IVCNZ.2016.7804442.
[40] W.H. Mosley, J. Bungey, Reinforced Concrete Design, 2 edition, The Macmillan Press Ltd, Kindon, 1982, https://doi.org/10.1007/978-1-349-16888-0. ISBN 978–1–349-16888-0.
[41] K. Nishio, Noriyoshi Nakamura, Yuta Muraki, K. Kobori, A method of core wire extraction from point cloud data of rebar, in: The 25th Internaional Conference in Central Europe on Computer Graphics, Visualization and Computer Vision 2016 in Co-Operation with EUROGRAPHICS, 2016, pp. 51–58. ISBN 978–80–86943-50-3. URL, https://dspace5.zcu.cz/bitstream/11025/29734/1/Nishio.pdf.
[42] Abdul Nurunnabi, David Belton, Geoff West, Robust segmentation for large volumes of laser scanning three-dimensional point cloud data, IEEE Trans. Geosci. Remote Sens. 54 (8) (2016) 4790–4805, https://doi.org/10.1109/TGRS.2016.2551546.
[43] Tarek Omar, Moncef L. Nehdi, Condition assessment of reinforced concrete bridges: Current practice and research challenges, Infrastructures 3 (3) (2018), https://doi.org/10.3390/infrastructures3030036. ISSN 2412-3811.
[44] Precast / Prestressed Concrete Institute, Tolerances for precast and prestressed concrete construction, in: Report, Precast / Prestressed Concrete Institute, 2000. URL, https://www.pci.org/PCI_Docs/Publications/PCI. Last accessed: 03/10/2021.
[45] Nisha Puri, Enrique Valero, Yelda Turkan, Frédéric Bosché, Assessment of compliance of dimensional tolerances in concrete slabs using tls data and the 2d continuous wavelet transform, Autom. Constr. 94 (2018) 62–72, https://doi.org/10.1016/j.autcon.2018.06.004. ISSN 0926-5805.
[46] Xianyu Qi, Wei Wang, Mei Yuan, Yuliang Wang, Mingbo Li, Lin Xue, Yingpin Sun, Building semantic grid maps for domestic robot navigation, Int. J. Adv. Robot. Syst. 17 (1) (2020), https://doi.org/10.1177/1729881419900066, 1729881419900066.
[47] Maria Rashidi, Masoud Mohammadi, Saba Sadeghlou Kivi, Mohammad Mehdi Abdolvand, Linh Truong-Hong, Bijan Samali, A decade of modern bridge monitoring using terrestrial laser scanning: Review and future directions, Remote Sens. 12 (22) (2020), https://doi.org/10.3390/rs12223796. ISSN 2072-4292.
[48] B. Riveiro, H. González-Jorge, M. Varela, D.V. Jauregui, Validation of terrestrial laser scanning and photogrammetry techniques for the measurement of vertical underclearance and beam geometry in structural inspection of bridges, Measurement 46 (1) (2013) 784–794, https://doi.org/10.1016/j.measurement.2012.09.018. ISSN 0263-2241.
[49] Standards Australia, AS5100 bridge design, URL, http://www.standards.org.au/, 2017. Last accessed: 14/09/2021.
[50] Standards Australia, As4671 Steel for the Reinforcement of Concrete, 2019. URL https://www.standards.org.au/standards-catalogue/sa-snz/building/bd-084/as-slash-nzs–4671-colon-2019. Last accessed: 14/09/2021.
[51] J. Tuley, N. Vandapel, M. Hebert, Analysis and removal of artifacts in 3-d ladar data, in: Proceedings of the 2005 IEEE International Conference on Robotics and Automation, 2005, pp. 2203–2210, https://doi.org/10.1109/ROBOT.2005.1570440. ISBN 1050–4729.
[52] U.S. Department of Transportation Federal Highway Administration, LTBP InfoBridge, URL, https://infobridge.fhwa.dot.gov/Home, 2020. Last accessed: 05/11/2021.
[53] Q. Wang, Yi Tan, Zhongya Mei, Computational methods of acquisition and processing of 3d point cloud data for construction applications, Arch. Computat. Meth. Eng. 27:pp (2020) 479–499, https://doi.org/10.1007/s11831-019-09320-4.
[54] Qian Wang, Automatic checks from 3d point cloud data for safety regulation compliance for scaffold work platforms, Autom. Constr. 104 (2019) 38–51, https://doi.org/10.1016/j.autcon.2019.04.008. ISSN 0926-5805.
[55] Qian Wang, Automatic checks from 3d point cloud data for safety regulation compliance for scaffold work platforms, Autom. Constr. 104 (2019) 38–51, https://doi.org/10.1016/j.autcon.2019.04.008. ISSN 0926-5805.
[56] Qian Wang, Min-Koo Kim, Applications of 3d point cloud data in the construction industry: a fifteen-year review from 2004 to 2018, Adv. Eng. Inform. 39 (2019) 306–319, https://doi.org/10.1016/j.aei.2019.02.007. ISSN 1474-0346.
[57] Qian Wang, Jack C.P. Cheng, Hoon Sohn, Automated estimation of reinforced precast concrete rebar positions using colored laser scan data, Computer-Aided Civil Infrastruct. Eng. 32 (9) (2017) 787–802, https://doi.org/10.1111/mice.12293.
[58] Seongheum Yoon, Qian Wang, Hoon Sohn, Optimal placement of precast bridge deck slabs with respect to precast girders using 3d laser scanning, Autom. Constr. 86 (2018) 81–98, https://doi.org/10.1016/j.autcon.2017.11.004. ISSN 0926-5805.
[59] Xinxing Yuan, Alan Smith, Rodrigo Sarlo, Christopher D. Lippitt, Fernando Moreu, Automatic evaluation of rebar spacing using lidar data, Autom. Constr. 131 (2021) 103890, https://doi.org/10.1016/j.autcon.2021.103890. ISSN 0926-5805.